Environmental Modelling and Software 143 (2021) 105117

Contents lists available at ScienceDirect

Environmental Modelling and Software

journal homepage: www.elsevier.com/locate/envsoft

A new modelling framework to assess biogenic GHG emissions from reservoirs: The G-res tool

Yves T. Prairie [a,*], Sara Mercier-Blais [a], John A. Harrison [b], Cynthia Soued [a], Paul del Giorgio [a], Atle Harby [c], Jukka Alm [d], Vincent Chanudet [e], Roy Nahas [a]

[a] UNESCO Chair in Global Environmental Change, Université Du Québec à Montréal, Montréal, Québec, Canada
[b] Washington State University, Vancouver, Vancouver, WA, USA
[c] SINTEF Energy Research, Trondheim, Norway
[d] Natural Resources Institute Finland, Joensuu, Finland
[e] Electricité de France, Hydro Engineering Centre, Risk and Sustainable Development Dpt, Le Bourget Du Lac, France

ARTICLE INFO

Keywords:
Carbon dioxide
Methane
Reservoir
G-res
Model
Greenhouse gas emission

ABSTRACT

Human-made reservoirs are now recognized as potentially significant sources of greenhouse gases, comparable to other anthropogenic sources, yet efforts to estimate these reservoir emissions have been hampered by the complexity of the underlying processes and a lack of coherent budgeting approaches. Here we present a unique modelling framework, the G-res Tool, which was explicitly designed to estimate the net C footprint of reservoirs across the globe. The framework involves the development of statistically robust empirical models describing the four major emission pathways for carbon-based greenhouse gases (GHG) from reservoirs: diffusive CO_2 and CH_4 emissions, bubbling CH_4 emissions from the reservoir surface, and CH_4 emissions due to degassing downstream the reservoir, based on an extensive meta-analysis of published data from the past three decades. These empirical models allow the prediction of reservoir-specific emissions, how they may shift over time and account for naturally occurring GHG generating pathways in aquatic networks.

1. Introduction

The creation of reservoirs by damming of rivers is one of the oldest and most profound landscape transformations exerted by humans. The inundation of a largely terrestrial ecosystem can radically change the carbon dynamics of the affected domain. Indeed, terrestrial systems are generally viewed as carbon sinks while freshwater ecosystems are most often sources of greenhouse gases (GHG) relative to the atmosphere (Borges et al., 2014; Cole et al., 2007; Raymond et al., 2013; Tranvik et al., 2009, Drake et al., 2018), with negative net ecosystem production (e.g. Ferland et al., 2014). This is the case because such systems often receive large amounts of organic carbon from the terrestrial ecosystems they drain and because the inland water network is a site for intense C processing. Unsurprisingly, freshwater reservoirs also emit GHGs, in many cases at higher areal rates than their natural counterparts (lakes and large rivers) because the flooded land under freshwater reservoirs provides a new source of organic matter available for decomposition and because it creates new environments conducive to the production of methane, a more potent GHG than CO_2.

Recent studies have concluded that the magnitude of GHG emissions from reservoirs can be of global significance. To date, most global assessments have simply used averages of measured values per climatic or geographic region that are then extrapolated worldwide. Although reasonable as a first order estimate, the validity of this approach rests on a number of implicit assumptions. For example, it assumes that the sampled systems are statistically representative of the global population of reservoirs. The accuracy of this method is also highly dependent upon the sampling strategy used to obtain reservoir-wide annual estimates, a potential shortcoming given the known large and highly skewed spatial and temporal variability of such estimates, both within and among reservoirs (Deemer et al., 2016; Deemer and Holgerson 2021; DelSontro et al., 2018a,b; Grinham et al., 2011; Prairie et al., 2018; Prairie et al., 2017; Rosentreter et al., 2021). Similarly, such an approach largely ignores the known temporal decrease in emission rates after flooding

* Corresponding author.
E-mail addresses: prairie.yves@uqam.ca (Y.T. Prairie), saramercierblais@gmail.com (S. Mercier-Blais), john_harrison@wsu.edu (J.A. Harrison), cynthia.soued@gmail.com (C. Soued), del_giorgio.paul@uqam.ca (P. Giorgio), atle.harby@sintef.no (A. Harby), jukka.alm@luke.fi (J. Alm), vincent.chanudet@edf.fr (V. Chanudet), roy.nahas@gmail.com (R. Nahas).

https://doi.org/10.1016/j.envsoft.2021.105117
Accepted 1 July 2021
Available online 7 July 2021

(Abril et al., 2005; Barros et al., 2011; Teodoru et al., 2012). Lastly, not all emissions occurring at the surface of reservoirs, specifically CO_2 emissions, should be considered new and attributable to impoundments since organic carbon loading from upstream catchments would sustain aquatic CO_2 emissions even in the absence of a reservoir (e.g., via CO_2 emissions from lakes, rivers, estuaries, or the coastal ocean).

Tools to quantify the current and future carbon footprint of reservoirs have not yet been developed, in part due to the complexity of the processes involved in generating reservoir GHG emissions, the multiple pathways through which GHGs are emitted from reservoirs (diffusion, ebullition and degassing), and the difficulty of accounting for pre-flooding GHG balances. Hindering the development of such tools is the fact that there have been only a handful of case studies that have quantified the complete C footprint of individual reservoirs (Teodoru et al., 2012; Abril et al., 2005), and these cannot be easily extrapolated to other sites. In spite of this, there have been a number of regional or global studies that have modelled specific aspects of reservoir C dynamics, such as CO_2 or CH_4 diffusive emissions (Barros et al., 2011; Deemer et al., 2016), but there is presently no platform that integrates the various aspects that make up the overall reservoir C footprint in a coherent and predictive context. To this end, we have developed an online modelling platform (hereafter the G-res Tool) that takes into account the specific environmental conditions of a reservoir to predict its associated emissions of both carbon dioxide (CO_2) and methane (CH_4), partition fluxes among the main emission pathways, and characterize the evolution of GHG fluxes over the expected lifetime of a given reservoir, here assumed to be 100 years. In addition, the G-res Tool estimates the GHG balance of the affected landscape prior to flooding, thereby allowing the estimation of the net GHG impact of reservoir creation by difference. The G-res Tool closely follows the conceptual approach outlined in Prairie et al. (2018), which ultimately aims at predicting the reservoir-induced change in GHG fluxes to the atmosphere of the flooded landscape. The G-res Tool is applicable globally (Harrison et al., 2021) and can be used with an Earth Engine functionality (Prairie et al., 2017) so that it can be used dynamically on existing reservoirs as well as on potential or planned reservoir locations.

The core of the G-res Tool relies on a series of empirical models developed from a synthesis of published literature on reservoir emissions. These models are based on the influence of local to regional environmental controls on GHG emission and on the characteristics of the individual reservoirs and their catchments. In this paper, we report on the development of the underlying models predicting the magnitude of each emission pathway, their linkages with global databases as well as their integration into a comprehensive and publicly available platform. In addition, to further validate ability to predict the temporal evolution of emissions in individual reservoirs, we compare model predictions with measured GHG fluxes in two of the most-studied reservoirs located in very contrasting climates (boreal and tropical) that were sampled extensively over a 12-year and 20-year period, respectively.

2. Methods

2.1.1. Modelling approach

The G-res Tool is designed to assess, in a comprehensive manner, the net GHG footprint of a reservoir over its lifetime (assumed to be 100 years, Gagnon et al., 2002; IAEA Advisoring Group, 1996; 1995), including the footprint associated with its construction. However, the present paper reports only on the biogenic components of the GHG balance of the reservoir area (i.e., without the construction), both prior to and after impoundment. The G-res Tool can therefore provide an estimate of the net GHG impact of reservoir creation. Similarly, the G-res Tool provides calculations to estimate the portion of GHG emissions that are likely the result of nutrient enrichment (so-called Unrelated Anthropogenic Sources, UAS (IPCC SRREN, Kumar et al., 2011), due to phosphorus inputs associated with human activities in the reservoir catchment. Based on the expected difference in phosphorus load in the absence of human-induced catchment perturbations (details of the approach can be found in the G-res Tool technical document, Prairie et al., 2017), the method is useful primarily in allocating reservoir GHG emissions to particular services or practices. However, emissions potentially attributable to UAS are not excluded from the present calculations of the GHG footprint of reservoirs and are therefore not addressed further in this paper (see Prairie et al., 2017 for further details).

2.2. Database

To develop the GHG emissions models, we undertook an extensive review of the pre-2016 scientific literature and collected data from 223 globally distributed reservoirs with CO_2 and CH_4 emissions measurements (279 field assessments of diffusive CO_2 emissions, 205 of diffusive CH_4 emissions, 59 of bubbling CH_4 emissions and 52 of degassing CH_4 emissions; See Supplementary material Figure S1 and Reference list and Prairie et al., 2017 and available at https://zenodo.org/record/4711132#.YOiwxy295oM). This database is largely overlapping with the one developed by Deemer et al. (2016). Because the assembled dataset of GHG emissions depended entirely on the availability of published data, we compared the size and climate distributions of the sampled reservoirs with that of a more exhaustive and larger set of reservoirs worldwide (GRanD database; Lehner et al., 2011). In general, our database essentially covered the full range of reservoir surface areas. Our dataset also covered all climate zones, although boreal (and to a lower extent sub-tropical and tropical) reservoirs were somewhat over-represented relative to the GRanD (See Supplementary material Table S2).

In addition to GHG flux data, we also collated information on climatic, geographic, edaphic and hydrologic conditions of each reservoir and its catchment. These variables were obtained from a variety of open sources including the literature, worldwide GIS layers (see Table 1) and information contained in the GRanD database (Lehner et al., 2011). The complete list of potential predictor variables from both reservoirs and catchments used in the models is listed in Table 1.

Geographical information systems (GIS) were used to acquire two sets of data, pertaining either to the reservoir themselves or their catchments. We used the GIS polygons provided in the GRanD database (156 reservoirs) when available and added 67 reservoirs that were delineated using contemporary satellite imagery. Zonal statistics tools applied to global raster layers were then used to estimate the variables of interests for each reservoir (e.g., soil carbon content, surface temperature, and wind speed). Similarly, the catchment dataset was built largely around the Hydrobasins GIS product (Lehner and Grill, 2013) to which was added several catchments that were delineated using the digital elevation model (DEM) of the shuttle radar topography mission (SRTM) and hydrological spatial analysis tools.

2.3. Standardization of data

2.3.1. Annualization

Since the GHG emissions data of the 223 reservoirs gleaned from the literature were sampled at different temporal scales (single time points, seasonal averages, annual averages), we standardized all the diffusive fluxes of CO_2 and CH_4 and the CH_4 bubbling flux extracted from the literature using a procedure that combined the annual temperature cycle at the reservoir location with the known temperature dependence associated with CO_2 and CH_4 production (Inglett et al., 2012; Liikanen et al., 2002; Yvon-Durocher et al., 2014; also see Prairie et al., 2017). For colder climates where reservoirs develop an ice cover, winter GHG accumulation under ice is accounted for by assuming that gas production occurs continuously at 4 degrees C, although it is likely that GHGs produced during ice cover are released during a short period (spring overturn). In brief, the procedure consisted of assigning a temperature to

Table 1
List of predictor variables used for modelling including the units to use, the source of data and supplemental information.

	Predictor Variables	Units	Source[a]	Supplemental information
Reservoir variables	Country		Literature, GRanD DB	
	Climate zone	–	Rubel and Kottek, 2010 Köppen-Geiger climate classification	4 categories compatible with the emission factor of IPCC (2006): Tropical, Subtropical, Temperate, Boreal
	Dam coordinates	DD	Literature, GRanD DB	
	Impoundment year		Literature, GRanD DB	
	Reservoir area	km^2	Literature, GRanD DB, GIS	
	Reservoir volume	km^3	Literature, GRanD DB	
	Maximum depth	m	Literature, GRanD DB, Estimated	Dam height used as a proxy of this value if unavailable
	Mean depth	m	Literature, GRanD DB, Estimated	Reservoir area and reservoir volume used in order to estimate this value if unavailable
	Thermocline depth	m	Literature, Estimated	Temperature, Reservoir area and Annual mean wind speed used in order to estimate this value if unavailable
	Littoral area	%	Literature, Estimated	Maximum and Mean depth used in order to estimate this value if unavailable
	Water residence time	yr	Literature, Estimated	Reservoir area, Mean depth, Catchment area and Annual runoff used in order to estimate this value if unavailable
	Mean monthly and annual air temperature	°C	Global Climate database (Hijmans et al., 2005)	Average for the period 1950–2000
	Annual precipitation	mm yr^{-1}	Global Climate database (Hijmans et al., 2005)	Average for the period 1950–2000
	Mean monthly and annual wind speed	m s^{-1}	NOAA GLOBE Task Team (Hastings et al., 1999)	
	Reservoir mean global horizontal radiance	kWh $m^{-2}d^{-1}$	SSE (NASA, 2008)	See Appendix A. To convert to Cumulative global horizontal radiance (kWh m^{-2} $period^{-1}$).
	Phosphorus concentration	µg L^{-1}	Literature, Estimated	Catchment land cover %, Catchment area, Water residence time and Annual runoff used in order to estimate this value if unavailable
	Soil carbon content of the inundated reservoir area	kgC m^{-2}	SoilGrids - global gridded soil information (Hengl et al., 2017)	Surface layer of the soil only (30 cm)
Catchment variables	Catchment area	km^2	Literature, GRanD DB, GIS	
	Mean annual runoff	mm yr^{-1}	Fekete et al. (2000)	
	Population density	person km^{-1}	CIESIN (2005)	
	Annual discharge	m^3 s^{-1}	Literature, Estimated	
	Land coverage	%	(ESA-CCI, 2014)	9 categories: Croplands, Forest, Grassland/Shrubland, Wetlands, Settlements, Bare Areas, Water Bodies, Permanent Snow/Ice, No Data

[a] Literature: Data from scientific publications, See Supplementary material Figure S1 and Reference list; GRanD DB: Data found in the GRanD DB (Lehner et al., 2011); Estimated: Using equation from the scientific literature (see Appendix A.); GIS: Data delineated using GIS spatial analysis, see section 2.1.

the observed GHG flux measurements and estimating the flux from the unsampled period by modulating the measured flux up or downwards using the temperature sensitivity metric appropriate for CO_2 ($Q_{10} = 2$, Inglett et al., 2012) and CH_4 ($Q_{10} = 4$, Yvon-Durocher et al., 2014). This method was applied for each unsampled month and all months were summed. This annualization procedure led to a modest adjustment downward for diffusive CH_4 emission (from an average 39.4 ± 152.5 measured flux to an average 33.5 ± 114.6 mg C m^{-2} d^{-1} annualized flux) because many measurements in regions with strong annual cycles were done exclusively in the summer months. However, the significantly reduced variability suggests that part of the initial noise in the collated data set was the result of sampling regime differences. Reservoirs with multiple years of measurements were used to evaluate the potential impact of reservoir aging on GHG emissions (Barros et al., 2011). If several independent measurements occurred at the same age, an average of all the measurements was calculated.

2.3.2. System-wide estimate of CH_4 ebullition

In most cases, CH_4 ebullition rates were reported either directly as system-wide estimates or as littoral-specific rates with the corresponding surface area. However, some studies reported littoral CH_4 ebullition rates without defining the surface the littoral zone encompassed. Since bubbling intensity is known to decrease with depth (Bastviken et al., 2008; DelSontro et al., 2010, DelSontro et al., 2011; Mcginnis et al., 2006) applying the littoral emission rates to the whole reservoir surface area would overestimate whole reservoir fluxes. To avoid this potential bias, for all studies reporting only littoral flux measurements, CH_4 ebullition flux rates were applied only to an area we defined as <3 m depth (see Appendix A from details) and then expressed as rates per unit surface area of the entire reservoir. We acknowledge that CH_4 bubbling can occur in some specific cases at greater depths (Mcginnis et al., 2006) and that this assumption may therefore result in an underestimate of reservoir-wide emissions. Nevertheless, given the physical inverse dependence of bubbling on depth (Bazhin, 2003) , we view this as an improvement over simply assuming littoral emissions rates occur over an entire reservoir's surface area at equal rates (Deemer et al., 2016).

2.3.3. Prioritization of data sources

For any given reservoir, several estimates of the same variables can be extracted from various sources. When such cases occurred, data gleaned directly from the scientific literature were prioritized for inclusion in the database, followed by the data from the GRanD database (Lehner et al., 2011). If values were unavailable from the peer-reviewed literature, we extracted the relevant values from global GIS layers (see Table 1) or estimated them from general models found in the literature (see Prairie et al., 2017 for details).

2.4. Statistical analysis and model development

Using the annualized GHG emission estimates described in section 2.2.1, we developed a series of multivariate statistical models to predict each flux pathway using both reservoir and catchment predictor variables. Variable selection was carried out using the elastic net regression procedure (see Prairie et al., 2017 for more details) implemented in JMP Pro 14 or 15. Elastic net regression is a penalty based variable selection method particularly well suited to modelling cases with a large number of potential predictor variables, even in cases with low sample size n (Zou and Hastie, 2005). The elastic net procedure reduces the variance

inflation problem associated with highly collinear variables by imposing a penalty on large coefficients. Depending on the penalty parameter, the algorithm can reduce regression coefficients to zero (i.e., no effect) thereby providing an objective variable selection procedure. Variable transformations (mostly logarithmic) were necessary to fulfill assumptions of the regression approach (e.g. normality of residuals) or desirability of the predictor variable distribution across their ranges. For each emission pathway, outliers were identified using Cook's distance (Cook, 1977) which combines the studentized residual and the observation's departure from the mean (using 3 times the mean, μ_D, as a threshold) and removed from the analysis.

2.4. Pre-impoundment GHG footprint

Large landscapes are generally a mosaic of ecosystems (forests, wetlands, cropland, settlements, lakes, streams, rivers, etc.) that all process carbon in different ways. Each of these ecosystems can emit or sequester carbon at different rates, contributing to the total carbon footprint of a defined area. For example, growing forests absorb CO_2 while wetlands tend to emit methane while sequestering CO_2. Soil type will also influence carbon processing, as organic soil will emit more GHG than mineral soil. Natural waterbodies, on the other hand, generally emit CO_2 and, to a lesser extent, methane. The pre-impoundment GHG balance of a reservoir area is therefore the weighted sum of the GHG balance of each landscape component. Because of the multiplicity of ecosystem types, we associated each landscape component within the impounded area with default CO_2 and CH_4 emission factors (EF) from the IPCC (IPCC, 2013). Specifically for the forest with mineral soils, we have used the default value from Pan et al. (2011) and for the methane emissions from water bodies, we used the equation developed in Rasilo et al. (2014) combined with appropriate gas exchange coefficients (Prairie et al., 2017; Vachon and Prairie, 2013). To follow the IPCC classification of EF, the top 30 cm of soil was assigned as mineral or organic soils using a threshold of 40 kg C m^{-2}, and the land impounded was associated to one of four climate zones: Tropical, Subtropical, Temperate and Boreal (Table 1). The general equation to estimate the pre-impoundment GHG balance was then:

$$\boldsymbol{Pre-impoundment GHG fooprint} = \sum_{j-1}^{2}\sum_{i-1}^{8}\left(EF_{LC.i} \times Area_{LC.i}\right) / Area_{reservoir} \quad (2)$$

where:

EF_{LC_ij} Emission factor specific to each land cover category and each gas (Prairie et al., 2017)
$Area_{LC\_i}$ Inundated area of each land cover category (km^2)
i Land cover category (8 categories, see Table 1)
j Pre-impoundment CO_2 or CH_4 emissions
$Area_{reservoir}$ Total reservoir area (km^2), including both existing river/lake area and inundated area

3. Results and discussion

3.1. Empirical modelling

For both CH_4 and CO_2 diffusive emissions, the age of the reservoirs was selected as one of the strongest predictors (as also found in Barros et al., 2011) and the regression equations therefore express emissions at a specific reservoir age. To evaluate the net footprint over the total lifetime of a reservoir, the non-linear regression equation was integrated using basic calculus to yield the 100-yr average annual emission rate (Equations 4 and 8, Table 2).

Methane emissions from reservoirs are more complex than CO_2 because three different pathways (degassing, bubbling and diffusion) can each deliver substantial amounts of CH_4 to the atmosphere and because each pathway is controlled by different drivers and must thus be modelled separately. The statistics of the four empirical models developed are detailed in Table 2.

3.1.1. CH_4 diffusive emissions

To predict diffusive CH_4 emissions, the elastic net procedure retained reservoir age, mean annual temperature, and percent littoral area (Table 2, Eq. 3) as the only useful predictors ($p < 0.0001$). The age of the reservoir had the strongest influence, particularly at high temperatures (Fig. 1a). Similarly, the decrease in GHG emission with age was strongest in reservoirs with extensive littoral zones (Fig. 1b). All three predictor variables confirmed trends previously reported in the literature for reservoirs and lakes (Barros et al., 2011; DelSontro et al., 2016; Liikanen et al., 2002; Yvon-Durocher et al., 2014).

3.1.2. CH_4 bubbling emissions

CH_4 is only sparingly soluble and can reach very high partial pressures when produced in sediments, leading to bubble formation when CH_4 partial pressure exceeds the sum of barometric and hydrostatic pressures. As bubbles grow larger or after a sudden change in pressure, bubbles can be released from the sediment into the water column, largely bypassing exchange within the water column (Mcginnis et al., 2006), and emitted directly to the atmosphere. Because of its dependence on hydrostatic pressure, the release of CH_4 bubbles is inversely proportional to water depth and, in many aquatic systems, confined to shallow zones in combination with areas of high sediment deposition.

A logarithmic equation using the cumulative global horizontal radiance (following the work of Wik et al., 2014) and percent littoral area as predictor variables was found to best represent CH_4 bubbling (reservoir-wide values). For CH_4 ebullition, the age of reservoir was not selected as a useful predictor by the elastic net regression procedure, which explains the absence of integrated model equation for this pathway (Table 2, Eq. 5). Given the limited number of bubble flux measurements ($n = 46$) and the wide confidence limits of the model, the emissions estimates associated with this pathway carry more uncertainty than the diffusive pathways (See Table 2). In this particular model, 4 observations were deemed outliers using the u*3 cook's distance criterion. Three of these systems were removed from the analysis, but we retained one (Eastmain-1 reservoir) because it represented one of the few points where the cumulative irradiance was low, thereby extending the model prediction range. Its inclusion did not affect the RMSE of the model but conferred more stability to the associated regression coefficient.

3.1.3. CH_4 degassing emissions downstream of reservoirs

Reservoir outflows can originate from various depths through various conduits (through turbines, spillways, bottom gates, and bypass channels), with important implications for CH_4 degassing fluxes. Deeper intakes are often preferred for hydropower stations for added operational flexibility. For thermally stratified systems or periods, drawing water from the hypolimnion can lead to high emission of methane downstream of a dam because high concentrations of CH_4 often accumulate in anoxic or sub-oxic hypolimnia. The sudden pressure drop after exiting a turbine can release a large fraction of the dissolved gas directly to the atmosphere, the so-called degassing process. CH_4-rich water drawn from a reservoir may also be released to the atmosphere in turbulent waters downstream the reservoir. Note that degassing emissions does not include these GHG emissions further downstream. This component is particularly difficult to predict given that methane oxidation can vary widely between ecosystems (Soued and Prairie, 2020; Thottathil et al., 2018, 2019).

Thus, a first requirement in assessing degassing emissions is to compare water intake and thermocline depths to determine whether water flowing downstream from dams is from the hypolimnion. If it is, it is likely to be CH_4-rich (leading to high degassing emissions). Conversely, if the water flows downstream from the epilimnion, it is

Table 2
The four (4) empirical models (in mg C $m^{-2}d^{-1}$or in t C yr^{-1}, for degassing). For models where Age of the reservoir is a predictor variable, equations are also provided to calculate the integrated emissions over the assumed lifetime of reservoirs (100 years) and represent the average areal rates over that period. The number of observations deemed outliers using Cook's D > 3 μ_D criterion were 15, 3, 2 and 3, respectively. RMSE is the Root Mean Square Error.

Predicted Variables	Empirical model equation	Equation number
CH_4 diffusive emissions (mg C $m^{-2}d^{-1}$) [a,b]	**At a specific age** $= 10^{\left(0.8032 - 0.01419 * Age + 0.4594 * log10\left(\frac{\%\ Littoral\ Area}{100}\right) + 0.04819 * Effective\ Temperature\ CH_4\right)}$ $R^2 = 0.51$ RMSE $= 0.52$ N $= 160$	*(3)*
	Integrated over lifetime (100yrs)[a] $= \frac{10^{\left(0.8032 + 0.4594 * log10\left(\frac{\%\ Littoral\ Area}{100}\right) + 0.04819 * Effective\ Temperature\ CH_4\right)} * \left(1 - 10^{(-(100 * 0.01419))}\right)}{(100 * 0.01419 * ln(10))}$	*(4)*
CH_4 bubbling emissions (mg C $m^{-2}d^{-1}$) [b,c]	$= 10^{\left(-1.3104 + 0.8515 * log10\left(\frac{\%\ Littoral\ Area}{100}\right) + 0.05198 * (Reservoir\ Cumulative\ Global\ Horizontal\ Radiance)\right)}$ $R^2 = 0.26$ RMSE $= 0.8$ N $= 46$	*(5)*
CH_4 degassing emissions (t Cyr^{-1}) [b]	$= \frac{10^{(-6.9106 + 2.950 * log10(CH4\ Diffusive\ Emissions\ Integrated\ on\ 100\ yrs) + 0.6017 * log10(WRT))} * 1000}{1000000000} * Catchment\ Area * 1000000 * \left(\frac{Annual\ Runoff}{1000}\right) * 0.9$ $R^2 = 0.68$ RMSE $= 0.81$ N $= 38$	*(6)*
CO_2 diffusive emissions (in mg C $m^{-2}d^{-1}$) [a, d]	**At a specific age** $= 10^{(1.860 - 0.330 * log10(Age) + 0.0332 * Effective\ Temperature\ CO_2 + 0.0799 * log10(Reservoir\ Area) + 0.0155 * Reservoir\ Surface\ Soil\ C\ Content + 0.2263 * log10(TP))}$ $R^2 = 0.36$ RMSE $= 0.39$ N $= 169$	*(7)*
	Integrated over lifetime (100yrs)[a] $= \left(10^{(1.860 + 0.0332 * Effective\ Temperature\ CO_2 + 0.0799 * log10(Reservoir\ Area) + 0.0155 * Reservoir\ Surface\ Soil\ C\ Content + 0.2263 * log10(TP))} * \frac{100^{(-0.330 + 1)} - 0.5^{(-0.330 + 1)}}{(-0.330 + 1) * (100 - 0.5)}\right)$	*(8)*

[a] The equation above uses the empirical model equation but also contains the operation necessary to integrate the emissions over 100 years (derived from calculus).
[b] Fluxes in CO_2e were derived using a global warming potential (GWP) of 34 over a 100-year period.
[c] See Appendix A for Reservoir Cumulative Global Horizontal Radiance calculation.
[d] Because of the logarithmic age term and the ensuing singularity at age = 0, the equation was integrated from 0.5 to 100 years.

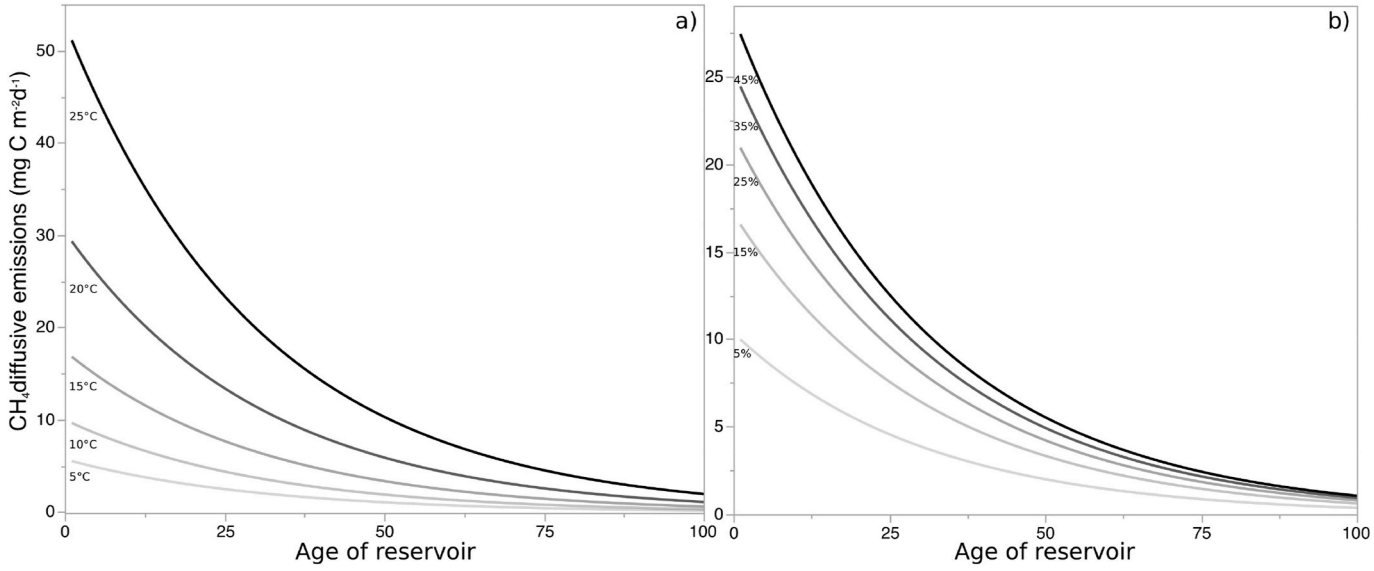

Fig. 1. Model-predicted changes in annual CH_4 diffusive emissions through time (years) for an average reservoir with a) littoral area of 24% and at several air temperatures; and b) a reservoir with a mean annual air temperature of 16.8 °C and for various littoral area.

likely to be comparatively CH_4-poor, leading to low degassing emissions. To account for this, the G-res Tool estimates degassing emissions only when the water intake is located below the thermocline.

To develop the G-res CH_4 degassing model, we calculated measured degassing flux as the difference in published CH_4 concentrations upstream and downstream of dams multiplied by mean annual flow through the turbines. We then tested for significant predictors of the difference between upstream (reservoir) and downstream CH_4 concentrations. The magnitude of these concentration differences was best predicted (Table 2, Eq. 6) as a function of water residence time (WRT) and post-impoundment annual CH_4 diffusive emission (itself estimated by the model described in section 3.1.1) as a proxy of CH_4 production. This provides an efficient method for predicting degassing emissions. Average discharge through the turbines was estimated as 90% of the annual runoff (as default value) although this value can vary substantially depending on the reservoir operations and maintenance.

3.1.4. CO_2 diffusive emissions

The best model for diffusive CO_2 flux, also determined using an elastic net regression procedure, includes reservoir age, mean annual temperature, modelled phosphorus concentration (Prairie et al., 2017), reservoir area and pre-inundation reservoir surface soil carbon content, as shown in Table 2 (Eq. 7). Because of the logarithmic nature of the relationship, negative CO_2 fluxes (i.e., reservoir acting as an atmospheric sink) are currently not included in the modelling. Persistent CO_2 influx is generally observed only under eutrophic conditions and/or when there are very low organic allochthonous carbon inputs (Soued and Prairie 2021). As a result, G-res can be construed as providing an upper limit to the CO_2 footprint of eutrophic systems. Compared to diffusive CH_4, the decline of CO_2 emissions over time is much steeper at first and stabilizes more quickly to a new equilibrium (Fig. 2). This temporal decrease has been reported in several cases (Abril et al., 2005; Demarty and Tremblay, 2017; Galy-Lacaux et al., 1997; Teodoru et al., 2012).

Predicted CO_2 diffusive emissions from both individual reservoirs and reservoirs collectively are highly influenced by temperature (Fig. 2a), and somewhat less sensitive to the amount of organic carbon contained in the flooded soil (Fig. 2b; Harrison et al., 2021), suggesting that diffusive CO_2 emissions from reservoirs could increase with increasing water temperatures anticipated to accompany ongoing climate change.

These models describe well both the main drivers and the temporal trajectory of CO_2 emissions and can therefore be used to estimate the expected emissions at any particular time post-flooding. Unlike CH_4 emissions (see Prairie et al., 2017), not all surface CO_2 emissions should be attributed to reservoir creation because, as with all inland aquatic systems, reservoir CO_2 emissions are also sustained by the mineralization (biological and photochemical) of allochthonous organic carbon (largely dissolved) originating from the upstream catchment. In the absence of a reservoir, allochthonous DOC would still have been mineralized to CO_2, albeit mostly further downstream. Furthermore, the longer water residence time of reservoirs relative to the river it replaced allows for more DOC mineralization to occur at the reservoir site (Algesten et al., 2005; Dillon and Molot, 1997; Vachon et al., 2017), exacerbating the magnitude of "displaced emissions" (sensu Prairie et al., 2017). The G-res Tool allows for an estimation of this portion of the CO_2 diffusive flux that can be legitimately attributed to the creation of a reservoir. To calculate this fraction, the G-res Tool assumes that the predicted CO_2 emission rate at year 100 post-flooding corresponds to naturally sustained emissions which are subtracted from the temporal trajectory to provide an estimate of the CO_2 attributable to mineralization of the flooded terrestrial biomass and soil C (see Prairie et al., 2017 for details). Under this assumption, the rate of decline through time (i.e. the Age variable coefficient in the regression model, −0.330) can be used to calculate that, over the 100-year lifetime of reservoirs, an average of about 31 (±6) % of the CO_2 emissions can be attributed to the impoundment, with the remaining being sustained by continuous allochthonous organic carbon.

The G-res platform also accounts for the CO_2 emissions from natural aquatic ecosystems located within the impoundment area prior to flooding. For example, when a lake is only slightly expanded by impoundment or when several lakes were submerged, G-res calculates reservoir CO_2 emission by applying the predicted areal rates (Eqs. 7 or 8) only to the newly flooded area rates using:

$$\textit{Newly impounded land ratio} = 1 - \frac{\%\ \textit{Water Body before impoundment}}{100} \tag{9}$$

3.2. Net GHG footprint

The sum of the 4 different components of emission gives the total post-impoundment emissions, from which the pre-impoundment emissions can be subtracted (or added) to obtain an estimate of the net GHG footprint (illustrated in the Graphical Abstract).

3.3. Validation

3.3.1. G-res modelling approach versus averages of measured values

The range of GHG emission rates found in the literature, regardless of emission pathway or ecosystem type, consistently shows a highly skewed distribution, with a few very high values, leading to mean values that are much higher than other measures of central tendency. By using log-transformed models, predictions from the G-res correspond to the geometric mean of the distribution of annualized, area-adjusted GHG flux measurements. However, because G-res relies on the main drivers of emissions from a set of local environmental factors through statistical relationships, it is less prone to overestimation than the often-used approach of simply applying the average value derived from a highly skewed set of measured fluxes to estimate the flux of unsampled reservoirs. To validate this claim, we used reservoirs for which CH_4 diffusive

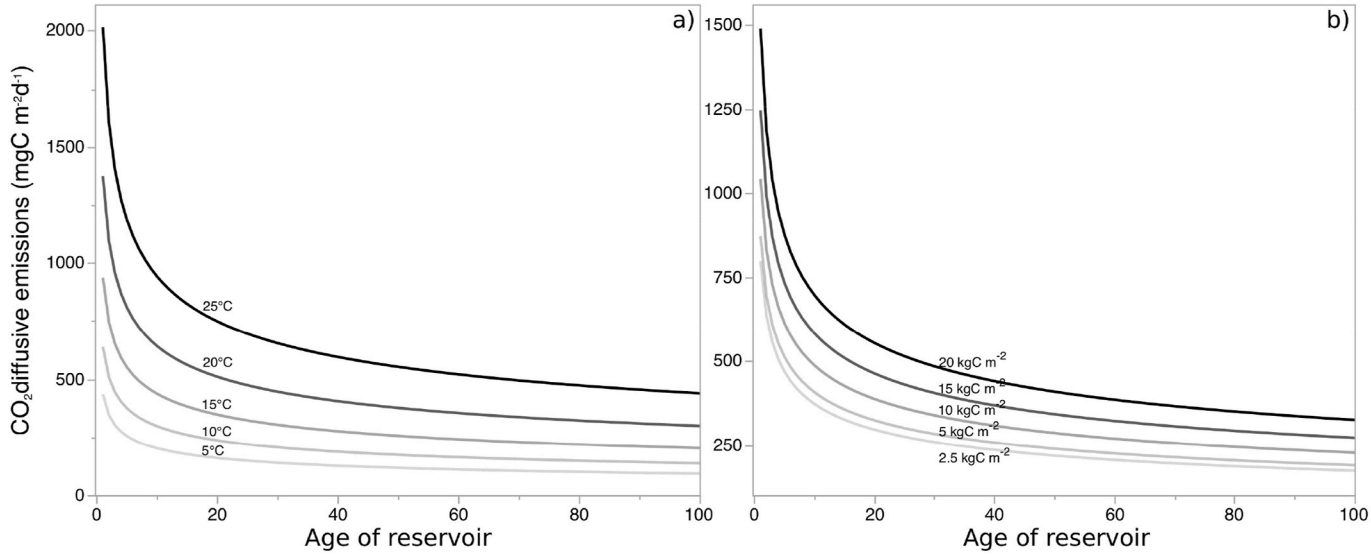

Fig. 2. Model-predicted changes in annual CO_2 diffusive emissions through time (years) for an average reservoir with a) a soil organic carbon content of 10.7 kgC m^{-2} and at several air temperatures; and b) a reservoir with a mean annual air temperature of 16.7 °C and for various soil carbon contents in the flooded soil.

emissions had been measured to compare the predictive ability of our G-res model estimation of reservoir-wide CH_4 diffusive emissions with those calculated by simply applying the average of all measured areal emission rates (38.5 mg C m^{-2} d^{-1}, from measurements used in this comparison) to the same systems. As expected, G-res predictions did not deviate significantly from the 1:1 line (Fig. 3a), while simply applying the observed mean to all reservoirs overestimated reservoir emissions in 84.1% of the cases and by an average of nearly an order of magnitude over the entire range of prediction (Fig. 3b). The corresponding Nash-Sutcliffe Efficiency statistics were 0.67 and 0.25, respectively. This underlines the importance of model-based predictions when dealing with highly skewed data. The same pattern was observed, albeit to a varying degree, when the individual pathways were examined separately (See Supplementary material Figure S2 and Table S1).

3.4. Emissions through time: the case study of two contrasting reservoirs

The general decline in GHG as a function of age of the reservoir observed in our models (Eq. 3 and 7) and reported elsewhere (Barros et al., 2011) is cross-sectional in nature, i.e., through the observations of different reservoirs of varying ages. To explore the longitudinal applicability of the models to individual reservoirs over time, we tested it to two well-studied but contrasting reservoirs from a boreal (Eastmain-1) and a tropical climate (Petit-Saut).

Eastmain-1, a 603 km^2 reservoir in the boreal region of Quebec (53°N), was flooded over the November 2005 to February 2006 period. The reservoir emissions were monitored and published in the scientific literature for seven (7) years after impoundment (year 2006–2009 (Bastien and Demarty, 2013; Demarty et al., 2009; Demarty and Tremblay, 2017; Teodoru et al., 2012; Tremblay et al., 2008; Tremblay et al., 2009), and further measured recently in 2018 (unpublished data, P. del Giorgio). Prior to flooding, the impounded area was dominated by forest (74%), with a small coverage of grassland/shrubland (10.5%), water bodies (11.5%) and wetlands (3%), and the impounded soils have organic carbon-rich content (22.3 kg C m^{-2} on average). This remote area has very limited human occupation or activities, and the reservoir is considered oligotrophic (total phosphorus concentration estimated by the G-res is 7.1 μg L^{-1} and measured as 9.3 μg L^{-1} in 2018 (unpublished data, P. del Giorgio).

In contrast, Petit-Saut is a tropical reservoir (4° N) located in French Guiana where 305.5 km^2 of forest (37%), wetlands (25.7%) and water bodies (32.9%) were flooded in 1994. The reservoir emissions were measured and published in the scientific literature for the first ten (10) years after impoundment (year 1994–2004, Abril et al., 2005), but were also continuously monitored in 2004–2014 (unpublished data, V. Chanudet). The impounded soil carbon content is 10.4 kgC m^{-2} on average and the reservoir is considered oligotrophic.

To compare Eastmain-1 observations with G-res Tool predictions, eight years of measurements for the ice-free period were annualized to account for the seasonal temperature cycle and corresponding GHG production (See section 2.2.1, Prairie et al., 2017b). For Petit-Saut, no such annualization was necessary given that measurements (monthly) were available from all seasons. For the purpose of this comparison, we did not distinguish between natural and anthropogenic CO_2 emissions (section 3.2.4, Prairie et al., 2017a,b). Also, because of the lack of time-series data on multiple GHG emission pathways, the comparison was only possible for CO_2 and CH_4 diffusive emissions.

For CO_2, Fig. 4a and b shows that both the magnitude and the decline in the rate of post-impoundment CO_2 emissions are, for the two contrasting reservoirs, reasonably well-predicted by G-res. As predicted, the initial emission rates were much higher in Petit-Saut than in Eastmain-1 Eastmain 1a but exhibited a similar rate of relative decline. Nevertheless, the model underpredicted emissions in the initial years at Eastmain-1 but G-res estimations and observations converged after a few years post-impoundment (Fig. 4a). For Petit-Saut, the G-res model predicted the initial rates quite well but tended to overestimate later on.

While the details of the temporal projections are important, the long-term cumulative footprint is particularly relevant given the overall purpose of the G-res platform. Fig. 4c–d illustrate how the estimated and observed cumulative CO_2 footprints track one another. For Eastmain-1, the G-res cumulative footprint was, on average 17%, lower that the cumulative observed CO_2 over the course of the observation period (12 years). For Petit-Saut, the cumulative CO_2 emission curve was nearly perfectly matched by G-res estimation (Fig. 4d).

For CH_4, the G-res model correctly predicted the one order of magnitude difference between diffusive CH_4 emission rates of the two reservoirs (Fig. 5). However, the temporal trends in measured emissions did not follow the G-res predicted rate of decline. For the tropical reservoir Petit-Saut, the observed decline was faster than predicted while the Eastmain-1 reservoir exhibited the reverse pattern (G-res predicted diffusive CH_4 flux to decline faster than it actually did). This suggests that, in its current form (Table 2, Eq. 3), the G-res CH_4 diffusive model apparently captures an average rate of decline but that the cross-sectional data was unable to detect the slower decline in very cold

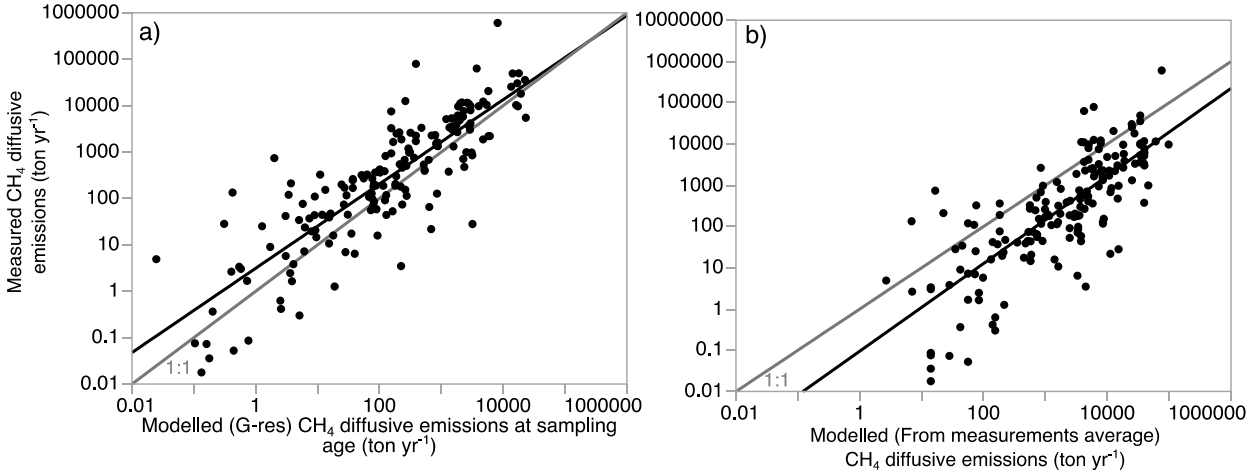

Fig. 3. Regression relationship of measured CH_4 diffusive emissions as a function of Modelled CH_4 diffusive emissions from the G-res model at sampling age (n = 176, R^2 = 0.72, Fig. 3a) and from applying the average areal rate to all reservoir surface (n = 176, R^2 = 0.61, Fig. 3b), black line. The grey lines correspond to line of equality (1:1).

environments and the steeper decline in tropical climates. This putative interaction between climate and the rate of temporal decline following impoundment can only be resolved by the incorporation of multiple long time-series of CH_4 from other reservoirs.

3.5. Uncertainty estimation

The G-res Tool ultimately aims at predicting the GHG footprint of reservoirs over their assumed lifetime (100 years) and therefore implies the integration over time of each of four statistical models summarized in Table 2. This operation is akin to estimating the long-term mean emission rate. As a result, we developed an uncertainty estimate to reflect the error variability of the estimated mean GHG footprint using Monte Carlo simulations. In brief, the predicted fluxes (log scale) from each emission pathway were contaminated randomly with normally distributed noise corresponding to the standard error of the residuals of each model and then summed after log de-transformation. We repeated the procedure to obtain 1000 estimates of the reservoir GHG emissions footprint from which we extracted the non-parametric 95% confidence limits. While these varied between reservoirs, the average lower and upper values corresponded to 87 and 120% of the mean. Note that if the G-res equations are instead used to estimate a reservoir's GHG footprint at a given age, uncertainty limits will be wider than for its lifetime integrated footprint and would require accounting for de-transformation bias.

3.6. G-res tool user interface

To make the predictive models described above widely available, we developed a web interface, hereafter called the G-res Tool. This online tool (www.hydropower.org/gres-tool) allows users to use reservoir-specific input data to calculate net GHG footprint estimates. The G-res Tool also provides auxiliary modules to estimate emissions for the construction phase as well as to allocate GHG footprint to the different services associated with a particular reservoir (Hydroelectricity, Water supply, Flood control, Irrigation, Fisheries, Recreation, Navigation and Environmental flow). The methods used in these modules are described in more detail in a technical document (Prairie et al., 2017). In this

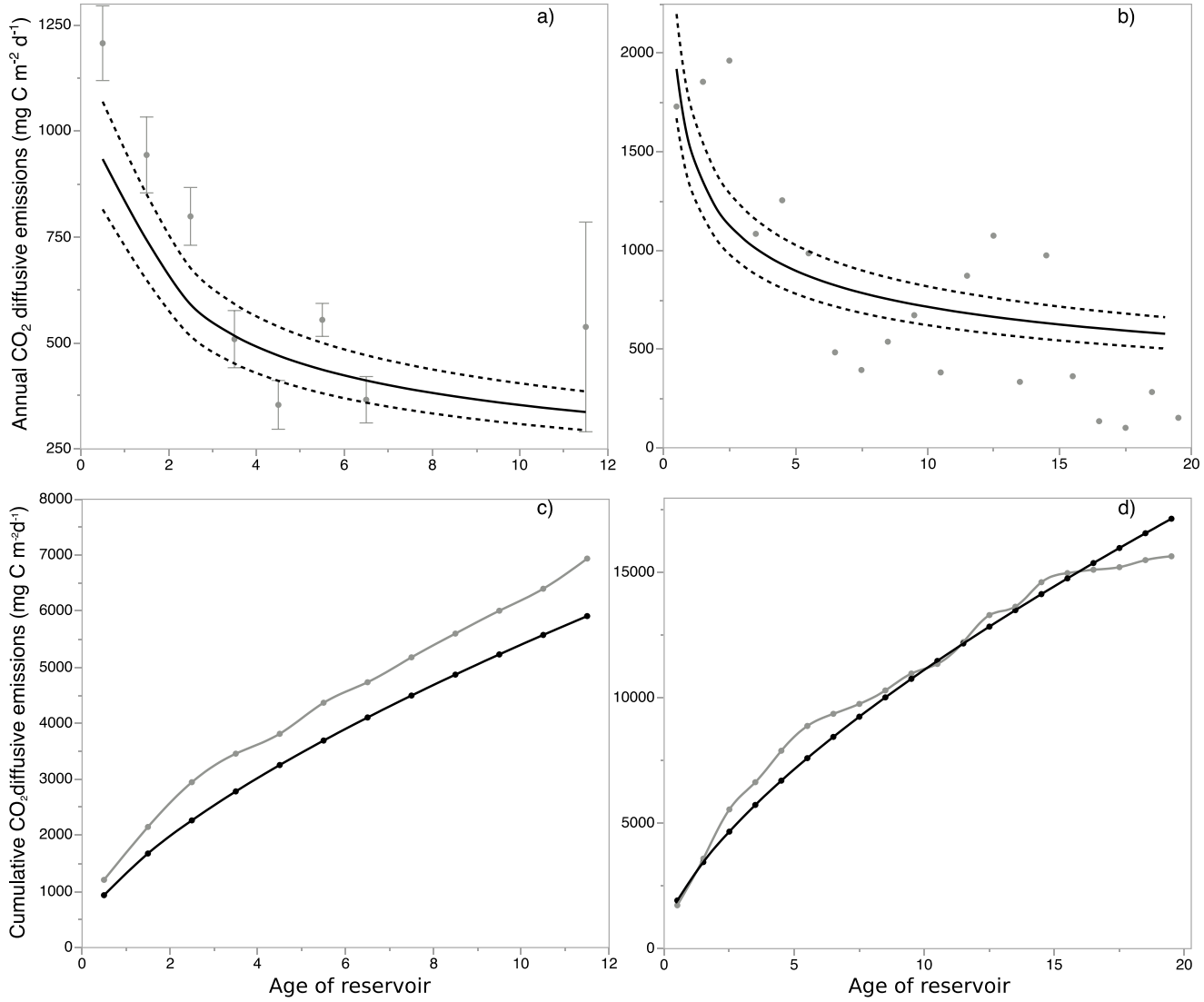

Fig. 4. G-res predicted Annual CO_2 emission values (mg C m^{-2} d^{-1}; Full black line) with model 95% confidence interval (dotted black line) compared to annualized field measurements diffusive CO_2 emissions (Grey points) with associated 95% confidence interval on the means (Grey bars) for reservoir measurements (12 yrs for Eastmain-1(a), 20 yrs for Petit Saut (c)) and Cumulative CO_2 diffusive emissions from G-res predicted values (Black) and Field measurement (Grey) for the 12 yrs measurements for Eastmain-1 (c) and 20 yrs for Petit Saut (d). Because no measurements were taken at Eastmain-1 during years 8–11 post-flooding, we calculated the cumulative CO_2 footprint series by using the fitted function (CO_2 emissions = 932.1 * $Age^{-0.368}$, r^2 = 0.61) for those missing years.

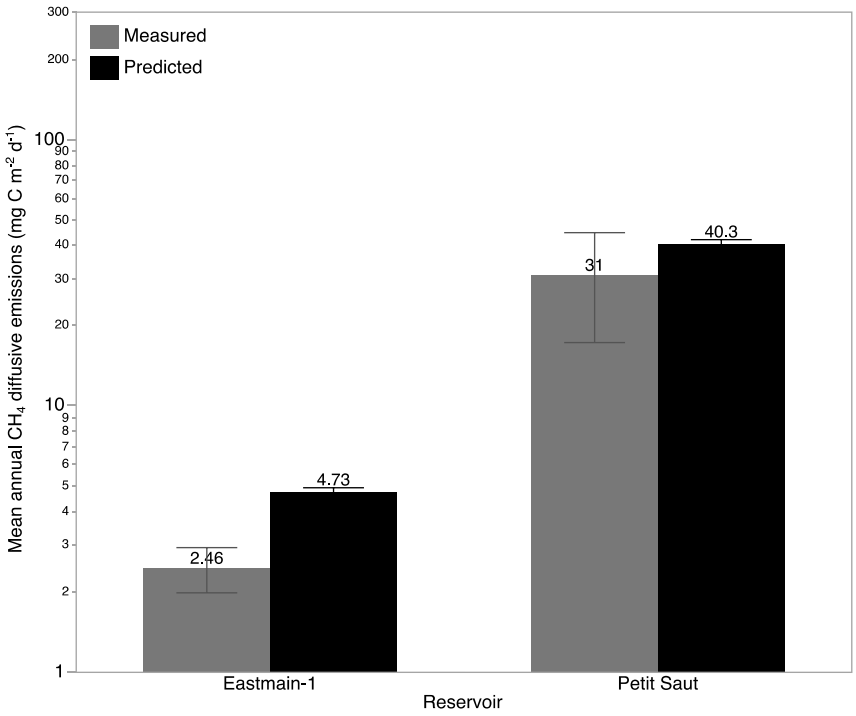

Fig. 5. Mean annual CH_4 diffusive emission values (mg C m^{-2} d^{-1}) predicted with the G-res model (Black) compared to mean field measurements (Grey) for the same period (12 years for Eastmain-1 and 20 years for Petit-Saut).

paper, we focus only on the pre- and post-flooding GHG balance of the reservoir area.

From the main Introductory G-res Tool web-page, nine other interacting tabs can be selected and used for several purposes, including: 1) entering input variables (about the reservoir and its catchment), 2) entering information about the usage of the reservoir (to allocate services), 3) entering information about the construction phase of the reservoir (to estimate construction-related GHG footprint), 4) viewing calculated reservoir post-impoundment GHG emissions, including the relative contribution of each emissions pathway and each GHG, the magnitude of unrelated anthropogenic sources, and an estimate of Total GHG flux (including an evaluation of the pre- and post-impoundment footprint), and 5) implementing a pre-programmed Earth Engine functionality to assist in obtaining all relevant and required input information from globally available and consistent sources (Prairie et al., 2017). This latter functionality can be used to obtain all required data by providing basic information (dam location, dam height) for existing reservoirs but can also be used to explore the GHG footprint of future or planned sites. Since the G-res Tool is cloud-based, the user can save input parameters locally and re-import them back in a subsequent use of G-res. Various report and export functions are available. Fig. 6 displays the main user interface outlook and the Total GHG footprint results page.

The G-res Tool has been available for use since 2017 (from version 1 onwards) and is now recommended by multiple stakeholders and international organizations with now more than 900 registered users and an average of 150 visits per month. While the G-res has been mostly used to estimate the carbon footprint of individual reservoirs, it has recently been used to estimate the biogenic GHG component in a Life Cycle Assessment of hydroelectricity generation for the whole province of Quebec (Levasseur et al., 2021). A further strategic importance of G-res lies in its ability to estimate GHG emissions for future projects, allowing better decision-making to build new reservoirs that have low carbon footprint. For example, estimates of high degassing emissions can lead to dam design changes (i.e. water intake depth) to reduce the importance of this pathway. Similarly, estimating the total GHG footprint is particularly important for banking institutions in their decision to finance future reservoir projects.

4. Discussion

4.1. Comparison to previous models

It is important to emphasize that there is currently no other modelling platform that can be used to compute, in a comprehensive and globally applicable framework, all four GHG emission pathways. The G-res integration of several components and flux estimates due to individual GHG emissions pathways moves beyond past efforts to quantify GHG emission from reservoirs (Barros et al., 2011; Bastviken et al., 2011; Deemer et al., 2016; Hertwich, 2013; St-Louis et al., 2000). Similarly, the ability to distinguish between natural and anthropogenic CO_2 emissions is unique to G-res as well as the estimation of the net GHG footprint through the estimation and accounting of the landscape GHG balance prior to flooding. Thus, the comparison between G-res and previously published models revolves around the driver variables identified, the extensiveness of the database used and, consequently, the robustness of the individual empirical models.

Barros et al. (2011) highlighted the influence of age and temperature (using latitude) on reservoir GHG emissions using 85 reservoirs. Similarly, the more recently published study from Deemer et al. (2016) has improved the estimation of GHG emissions from reservoirs by using a much bigger database (267 reservoir-years, largely overlapping with ours), as well as showing that reservoir productivity plays an important role in GHG emissions, along with age, temperature and hydrology. The G-res model developed here builds on these studies and has confirmed many of these drivers previously identified while integrating several new ones to develop a globally consistent modelling platform for each component of reservoir GHG emission based on a much larger number of potential predictor variables (>40; see Table 2 for the variables retained). The incorporation of the more recently available GHG measurements into empirical models has improved predictive power and, in particular, the robustness of the estimated model coefficients. For

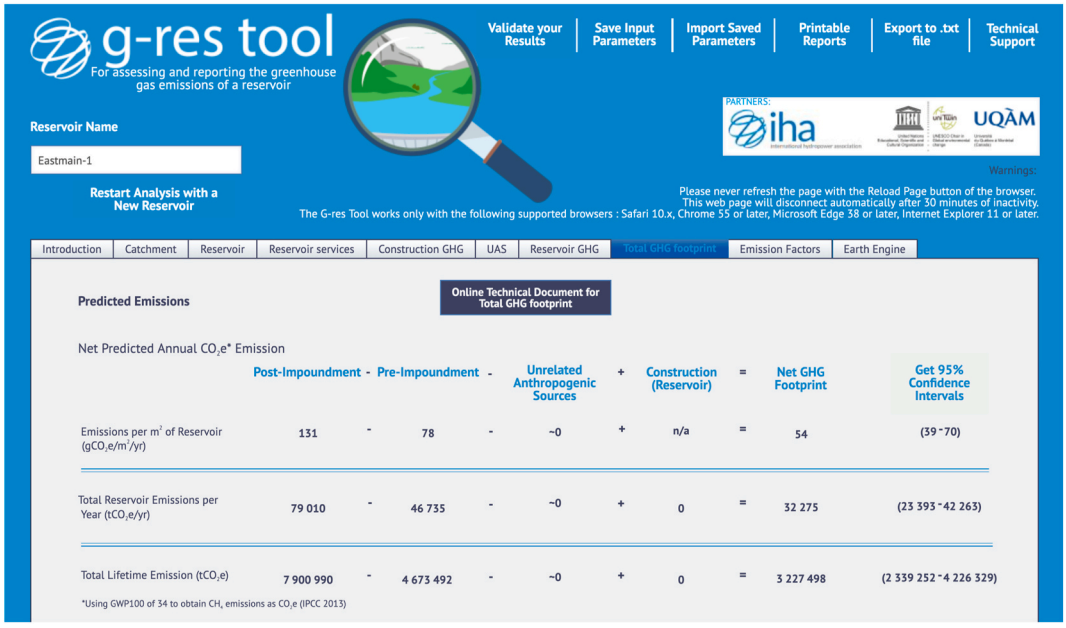

Fig. 6. G-res Tool web interface v 2.1 Total GHG footprint results page showing Post-Impoundment, Pre-Impoundment, UAS, Construction emissions and the Net GHG footprint of the reservoir (with 95% confidence intervals) in three different units: emissions per m^2 of reservoir ($gCO_2e\ m^{-2}\ yr^{-1}$), total reservoir emissions per year ($tCO_2e\ yr^{-1}$) and total lifetime emissions (tCO_2e).

models where the age of the reservoir was deemed a significant predictor (diffusive CO_2 and CH_4 emissions), the larger dataset helped better define the temporal evolution of emissions and therefore the integrated lifetime (100 years) GHG footprint, also a unique feature of G-res. While their predictive abilities are far from perfect, regression-based models are also less prone to introduce biases than a simple application of average per-area rates, particularly in the case of GHG pathways (mostly for CH_4) known to have a highly skewed distribution. For example, regional or global estimates of GHG emissions from reservoirs derived from simply applying an average value inherently assumes that the sampled systems are representative of the population distribution. Validation of the G-res models provided in this study (Fig. 4) illustrates that the regression-based approach can considerably reduce biases.

Another important feature unique to the G-res modelling platform is that it can provide estimates of so-called displaced emissions of CO_2, i.e. emissions that take place at the reservoir surface that are sustained by upstream loading of organic carbon mineralized within the reservoir but that would have occurred regardless of the presence of the reservoir, albeit elsewhere downstream in the hydrological network (Section 3.1.4, *sensu* Prairie et al., 2018).

4.2. Partitioning among emission pathways

The heterogeneity of the modelling database precluded the direct comparison of the relative importance of the various GHG components because very few reservoirs had concurrent measurements of all emission pathways. However, the modelled emission rates to the same dataset shows that, excluding the CH_4 degassing component, the overall GHG footprint is dominated by the CO_2 diffusion pathway in about 73% of the cases while CH_4 diffusion and bubbling is the main pathway in 10 and 16% of the reservoirs, respectively (See Supplementary material Figure S3). In this analysis, CH_4 degassing was omitted because its contribution to the overall GHG footprint was relatively small (mean: 14%, median: 4%) and it would assume that all reservoirs have the required configuration for significant degassing to occur (i.e. hydropower reservoirs with deep water intake). Note that these numbers apply specifically to the dataset assembled here and can differ in a more global context (Harrison et al., 2021).

4.3. Limitations of the models

While the G-res model predictions carry large numerical uncertainty, the G-res Tool is, to our knowledge, the most complete and the only globally consistent framework to predict the GHG footprint of reservoirs. However, proper usage of G-res also requires an understanding of its current limitations. For example, because the models are regression-based, one of the inherent limits of application is the observation range in the predictor variables of the assembled model dataset. While the observational ranges in our dataset captures most the variability of the global database provided in the GRanD database (Lehner et al., 2011) (Table S2), we recommend applying G-res only to reservoirs that fall within the limits of the current data. Furthermore, the G-res development has helped identify a number of knowledge gaps that deserve additional attention and research. These include: 1) the impact on GHG fluxes of reservoir location, operation and water transfers between reservoirs and power plants within watersheds, 2) the potential for reservoirs to act as GHG sinks, 3) newly identified flux pathways, 4) potential carbon burial in sediments and 5) the impact of eutrophication on reservoir GHG emissions.

The first important element not considered in the G-res framework is the prediction for cascade systems, where outflow from one reservoir (or a series of reservoirs) flows into one or more reservoirs further downstream. At present, reservoirs are considered independent and G-res therefore assumes that carbon processing in one reservoir does not affect that of downstream reservoirs. There is very little empirical information in the scientific literature on whether this assumption is reasonable. However, given that part of the allochthonous organic carbon input to the first reservoir of a cascade will be mineralized and lost from the hydrological system, one would hypothesize that at least the CO_2 emission in a downstream reservoir is likely to be lower than it would have been in the absence of a reservoir upstream. CH_4 emissions are less likely to be affected by upstream conditions since they result largely from the creation of new anoxic environments (Liu et al., 2020). Nevertheless, given that systems of cascading reservoirs and inter-basin transfers are common in many areas of the world, measurement

campaigns aiming to test these hypotheses would be useful.

Another area that would benefit the development of more robust CO_2 models is the ability to quantify reservoirs with negative diffusive CO_2 fluxes (i.e., where reservoirs act as CO_2 sinks). The logarithmic nature of our models is not well-suited for this purpose. While not common, CO_2 uptake has been observed (Chanudet et al., 2011), generally in eutrophic reservoirs although recent report shows that it can also occur periodically in oligotrophic conditions with very low organic carbon concentrations (Soued and Prairie 2021). It also highlights that predicting CO_2 fluxes sustained by allochthonous input is paramount to the accurate estimation of the true CO_2 footprint of reservoirs. A related limitation of the current G-res version is the absence of an explicit carbon sedimentation component. Cases of persistent negative fluxes indicate reservoirs that necessarily accumulate carbon, through sedimentation and burial. Recent measurements have shown that sediment carbon accumulation can be large in reservoirs (Mendonça et al. 2014, 2017). While the ensuing carbon accumulation cannot, from a mass-balance perspective, be simply subtracted from the flux at the air-water interface (see Prairie et al., 2017 for details) to obtain a net footprint, there are circumstances in which a portion of the carbon burial can be construed as a new sink (Isidorova et al., 2019), i.e. carbon burial that would not otherwise occur either at the reservoir site or further downstream. There are currently too little data to estimate the portion of the carbon accumulation that can be rightfully considered a new sink but future versions of G-res and other, yet-to-be-created, reservoir GHG models should incorporate this pathway to offer a more complete representation of the reservoir GHG footprint.

Another limitation of the current G-res model is that new emission pathways are being identified but for which observations are too few and therefore difficult to generalize. Identified nearly two decades ago (Fearnside 2002), recent studies have suggested that GHG fluxes from drawdown zones can be important although highly variable because they depend, in part, on the carbon and moisture content of the exposed soil/sediments (Marcé et al., 2019; Serça et al., 2016). Such emissions have been shown to be very high in some systems (Amorim et al., 2019). Given the paucity of literature on the subject, the emissions from drawdown areas are not explicitly included in G-res (although assumed implicitly to be of same magnitude as surface flux since G-res uses the maximum surface of the reservoir in the footprint calculations). Similarly, assessments of degassing emissions have been largely confined to CH_4 although CO_2 is known to be also emitted through this pathway. However, as additional data become available, GHG emissions from these pathways should be modelled explicitly and integrated in future iterations of G-res.

Another improvement would be the incorporation of an explicit representation of the relationship between GHG emissions and trophic status. Recent analyses have reported strong, positive correlations between CH_4 emissions and lake trophic status both within single lakes across time and space (Grinham et al., 2018; Li et al., 2018) and in multiple-lake syntheses (Beaulieu et al., 2019; Deemer et al., 2016; DelSontro et al., 2018; Harrison et al., 2017). A positive relationship between primary production and CH_4 emissions makes sense as organic matter can stimulate CH_4 production as an organic substrate for acetoclastic CH_4 production, and it can also foster the anaerobic conditions necessary for CH_4 production (and inhibit CH_4 oxidation). Limited experimental work has also indicated a relationship between CH_4 production and organic C quality (West et al., 2016). Intriguingly, recent work also shows that direct production of CH_4 in oxic surface waters by cyanobacteria could strongly link primary production and CH_4 emissions (Bižić et al., 2020), although the importance of this process in controlling CH_4 emissions is under debate (Günthel et al., 2021; Peeters and Hofmann 2021). Furthermore, future emissions are likely to be sensitive to changes in organic C delivery (Bayer et al., 2019). To-date, the absence of global-scale information on Chl *a* concentrations or trophic status has precluded the effective incorporation of such a driver in the global G-res model. However, efforts are underway to develop such information, and it may soon be possible to include such information in a global reservoir GHG model. As eutrophication may often be linked to UAS loading (see 2.1.1), improving the incorporation of the relationship between GHG emissions and trophic state will also be useful for identifying the impact of UAS.

Lastly, the net GHG footprint, i.e., the difference in the GHG balance before and after impoundment, currently relies on generic CH_4 and CO_2 emissions factors from the IPCC for different land cover types in different climate zones. Application of our current approach to our modelling dataset suggests that, while significant in areas where the flooded terrestrial landscape is rich in highly organic soils or if the flooded land has special characteristics leading to large fluxes of GHG, the importance of the GHG balance of the pre-flooding landscape is generally modest, altering the median footprint by only 4%. While a useful first order approach, we fully acknowledge that further improvements will require a more explicit modelling approach to the GHG balance of the individual components of the terrestrial mosaic in place before flooding.

5. Conclusion

The G-res model framework proposes a novel integrative approach to the prediction of Net GHG footprint from reservoirs whereby predictions include the local environmental conditions and physical configuration of each reservoir in a globally consistent predictive framework. It allows for a quantification of relative contribution of various emission pathways of CH_4 and CO_2 and how emissions of these gases change over time after impoundment. Accounting for temporal trends provides a means to assess its GHG footprint over the lifetime of reservoirs and also the estimation of the share of CO_2 emissions that are sustained by external organic inputs that would have occurred even in the absence of the reservoir, the so-called displaced emissions (Prairie et al., 2018).

The G-res Tool and associated models are freely available in a cloud-based modelling portal that will allow the scientific community to further probe the past and future geography of carbon emissions from reservoirs by applying the framework to larger datasets than the one used to develop it. The framework and its components will continue to evolve as new data become available that allow for the core models to be extended and improved, as new information on reservoir functioning emerges, and as users provide feedback and insight on its structure and components.

In a changing world where assessing GHG emissions of projects such as reservoir creation becomes standard practice, such a tool will be essential for decision makers to quantitatively evaluate alternative projects in order to select those with the lowest possible environmental footprints. The tool could also help in locating and designing new dams and their corresponding reservoirs, in guiding the operation of existing reservoirs, and in the potential retro-fitting of existing hydropower plants and dams to reduce GHG emissions.

Declaration of competing interest

The authors declare that they have no known competing financial interests or personal relationships that could have appeared to influence the work reported in this paper.

Acknowledgements

The G-res Tool was developed with the financial support of the International Hydropower Association and from the WorldBank. Special thanks to Rikard Liden, Richard Taylor and Mathis Rogner for many discussions. Further funding to YTP was provided by the NSERC Discovery grant. This is a contribution to the UNESCO Chair in Global Environmental Change. Funding to JAH was provided by an NSF INFEWS grant (NSF EAR1639458), a GRIL Fellowship grant, the Cox visiting professorship fund at Stanford University, a U.S. Army Corps of

Engineers Climate Preparedness and Resilience Programs grant, and a NSF DEB Grant #135211.

Appendix A. Supplementary data

Supplementary data to this article can be found online at https://doi.org/10.1016/j.envsoft.2021.105117.

Appendices.

A. Additionnal equations used

A.1. Air Density (kg/m^3)

$$Air\ Density = \frac{101325}{287.05 * (Mean\ Temperature\ of\ the\ 4\ Warmer\ Months + 273.15)}$$

A.2. Bottom Temperature (°C)

- If *Mean Temperature of the Colder Month* > 1.4:

$$Bottom\ Temperature = 0.656 * Mean\ Temperature\ of\ the\ Colder\ Month + 10.7$$

- If *Mean Temperature of the Colder Month* ≤ 1.4:

$$Bottom\ Temperature = 0.2345 * Mean\ Temperature\ of\ the\ Colder\ Month + 10.11$$

A.3. Bottom Water Density (kg/m^3)

$$Bottom\ Water\ Density = \left[1 - \frac{Bottom\ Temperature + 288.9414}{508929.2 * (Bottom\ Temperature + 68.12923)} * (Bottom\ Temperature - 3.9863)^2\right] * 1000$$

A.4. Surface Temperature (°C)

$$Surface\ Temperature = Mean\ Temperature\ of\ the\ 4\ Warmer\ Months$$

A.5. Surface Water Density (kg/m^3)

$$Surface\ Water\ Density = \left[1 - \frac{Surface\ Temperature + 288.9414}{508929.2 * (Surface\ Temperature + 68.12923)} * (Surface\ Temperature - 3.9863)^2\right] * 1000$$

A.6. CD

$$CD = If\ (Reservoir\ Mean\ Wind\ Speed < 5\ ;\ 0.001\ ;\ 0.000015\ )$$

A.7. Annual Wind Speed at 10m (m/s)

$$Annual\ Wind\ Speed\ at\ 10\ m = Reservoir\ Mean\ Wind\ Speed\ at\ X\ m * \left(1 - \left(\frac{CD^{0.5}}{0.4}\right) * Log\ 10\left(\frac{10}{X}\right)\right)^{-1}$$

**X equal 50 m in our database.

A.8. Reservoir Volume (km^3)

$$Reservoir\ Volume = Reservoir\ Area * (Mean\ Depth\ /\ 1000)$$

A.9. Reservoir Area (km^2)

$$Reservoir\ Area = \frac{Reservoir\ Volume}{Mean\ Depth/1000}$$

A.10. Mean Depth (m)

$$Mean\ Depth\ =\ Volume/Reservoir\ Area*1000$$

A.11. Thermocline Depth (m)

$$Thermocline\ Depth = 2.0*\sqrt{\frac{CD*Air\ Density*Annual\ Wind\ Speed\ at\ 10m^2}{9.80665*(Bottom\ Water\ Density - Surface\ Water\ Density)}}*\sqrt{\sqrt{Reservoir\ Area}}*1000000$$

**(Gorham and Boyce, 1989).

A.12. Temperature Correction Coefficient CH_4 (To do for Each Month)

$$Temperature\ Correction\ Coefficient\ CH_4 = 10^{(Temperature\ per\ Month*0.052)}$$

** 0.052 is the slope of the temperature vs CH_4 flux function in our database.
** If Temperature per month lower then 4 °C, use 4 °C.

A.13. Temperature Correction Coefficient CO_2 (To do for Each Month)

$$Temperature\ Correction\ Coefficient\ CO_2 = 10^{(Temperature\ per\ Month*0.05)}$$

** 0.05 is the slope of the temperature vs CO_2 flux function in our database.
** If Temperature per month lower then 4 °C, use 4 °C.

A.14. Effective Temperature CH_4(°C)

$$Effective\ Temperature\ CH_4\ = \frac{log10(Average\ (12\ Month\ Temperature\ Correction\ Coefficient\ CH_4\ ))}{0.052}$$

** 0.052 is the slope of the temperature vs CH_4 flux function in our database.

A.15. Effective Temperature CO_2 (°C)

$$Effective\ Temperature\ CO_2 = \frac{log10(Average\ (12\ Month\ Temperature\ Correction\ Coefficient\ CO_2\ ))}{0.05}$$

** 0.05 is the slope of the temperature vs CO_2 flux function in our database.

A.16. k600

$$k600\ =\ 0.24\ *\ (\ 2.51 + 1.48\ *\ Annual\ Wind\ Speed\ at\ 10m^2 + 0.39\ *\ Annual\ Wind\ Speed\ at\ 10m^2\ *\ log\ (\ Reservoir\ Area))$$

** Vachon and Prairie (2013).

A.17. kh

$$kh\ =\ exp\ (\ (\ -115.6477\ -\ 6.1698\ *\ (Effective\ Temperature\ CH_4\ +\ 273.15)\ /\ 100\ )\ +\ (155.5756\ /\ ((Effective\ Temperature\ CH_4\ +\ 273.15)\ /\ 100)\ )\ +\ (\ 65.2553\ *\ ln\ ((Effective\ Temperature\ CH_4\ +\ 273.15)\ /\ 100))\ *\ (\ 1000\ /\ 18.0153\ )$$

** (Lide, 1994).

A.18. pCH_4

$$pCH_4 = 10^{(\ (\ 1.46\ +\ 0.03\ *\ Effective\ Temperature\ CH_4)\ -\ 0.29\ *\ log\ (Reservoir\ Area)\ )}$$

** Rasilo et al. (2014).

A.19. Surface Water CH_4 Concentration

$$Surface\ Water\ CH_4\ Concentration = kh\ *\ pCH_4$$

A.20. CH_4 Emission Factor for Water Bodies (kg CH4/ha/yr)

$$CH_4\ Emission\ Factor\ for\ Water\ Bodies\ =\ Surface\ Water\ CH_4\ Concentration\ *\ k600\ *\ 16\ *\ \frac{365}{100}$$

A.21. q-bathymetric Shape

$$q-bathymetric\ shape = \frac{Maximum\ Depth}{Mean\ Depth}\ -\ 1$$

A.22. % Littoral Area

$$\%\ Littoral\ Area = \left(1-\left(1-\frac{3}{Maximum\ Depth}\right)^{q\ -\ bathymetric\ \ shape}\right)*100$$

A.23. Phosphorus Load - Forest (kg/ha/yr)

$$Phosphorus\ Load\ factor\ -\ Forest\ =\ \frac{10^{\left(0.914\ -\ log10\left(\left(\frac{Catchment\ \ Land\ \ Cover\ \%\ -\ Forest}{100}\right)\ *\ Catchment\ \ Area\right)\ *\ 0.014}}{100}$$

A.24. Phosphorus Load - Croplands (kg/ha/yr)

$$Phosphorus\ Load\ factor\ -\ Croplands\ =\ \frac{10^{\left(1.818\ -\ log10\left(\left(\frac{Catchment\ \ Land\ \ Cover\ \%\ -\ Croplands}{100}\right)\ *\ Catchment\ \ Area\right)\ *\ 0.227}}{100}$$

A.25. Population in the Catchment (person)

$$Population\ in\ the\ Catchment = Catchment\ Area * Population\ Density$$

A.26. Annual discharge (mm/yr)

$$Annual\ Discharge = Annual\ Runoff\ *\ 0.001\ *\ Catchment\ Area * 1000000/31536000$$

A.27. Water Residence Time (WRT, yrs)

$$WRT\ =\ \frac{Mean\ Depth * Reservoir\ Area}{Catchment\ Area * Annual\ Runoff} * 1000$$

A.28. River Area Before Impoundment (km^2)

$$River\ Area\ Before\ Impoundment = \frac{River\ Length\ Before\ Impoundment * 5.9 * Catchment\ area^{\ 0.32}}{1000000}$$

A.29. Reservoir Cumulative Global Horizontal Radiance (kWh/m^2/period)

- If 40 > Latitude > −40:

$$Reservoir\ Cumulative\ Global\ Horizontal\ Radiance = (Average\ (12\ Month\ Reservoir\ Mean\ Global\ Horizontal\ Radiance) * Number\ of\ month\ over\ 0^{\circ}C)$$

- If 40 < Latitude

$$Reservoir\ Cumulative\ Global\ Horizontal\ Radiance = (Average\ (May;\ June; July; August; September\ Reservoir\ Mean\ Global\ Horizontal\ Radiance) * Number\ of\ month\ over\ 0^{\circ}C)$$

- If - 40 > Latitude

Reservoir Cumulative Global Horizontal Radiance = (*Average* (*November*; *December*; *January*; *February*; *March Reservoir Mean Global Horizontal Radiance*) * *Number of month over* $0^{\circ}C$)

References

Abril, G., Guérin, F., Richard, S., Delmas, R., Galy-Lacaux, C., Gosse, P., et al., 2005. Carbon dioxide and methane emissions and the carbon budget of a 10-year old tropical reservoir (Petit Saut, French Guiana). Global Biogeochem. Cycles 19 (GB4007), 1–16. https://doi.org/10.1029/2005GB002457.

Algesten, G., Sobek, S., Bergström, A.-K., Jonsson, A., Tranvik, L.J., Jansson, M., 2005. Contribution of sediment respiration to summer CO2 emission from low productive boreal and subarctic lakes. Microb. Ecol. 50 (4), 529–535. https://doi.org/10.1007/s00248-005-5007-x.

Amorim, M., Aurélio, M., Marcello, J., Camargo, R. De, 2019. Methane diffusive fluxes from sediment exposed in a Brazilian tropical reservoir drawdown zone. J. S. Am. Earth Sci. 90, 463–470. https://doi.org/10.1016/j.jsames.2018.12.025.

Barros, N., Cole, J.J., Tranvik, L.J., Prairie, Y.T., Bastviken, D., Huszar, V.L.M., et al., 2011. Carbon emission from hydroelectric reservoirs linked to reservoir age and latitude. Nat. Geosci. 4 (9), 593–596. https://doi.org/10.1038/ngeo1211.

Bastien, J., Demarty, M., 2013. Spatio-temporal variation of gross CO2 and CH4 diffusive emissions from Australian reservoirs and natural aquatic ecosystems, and estimation of net reservoir emissions. Lakes Reservoirs Res. Manag. 18, 115–127. https://doi.org/10.1111/lre.12028.

Bastviken, D., Cole, J., Pace, M., Van de Bogert, M., et al., 2008. Fates of methane from different lake habitats: connecting whole-lake budgets and CH4 emissions. Journal of Geophysical Research 113 (G2). https://doi.org/10.1029/2007JG000608.

Bastviken, David, Tranvik, L.J., Downing, J., Crill M, P., J. a, Enrich-Prast, A., 2011. Freshwater methane emissions offset the continental carbon sink. Science 331, 50. https://doi.org/10.1126/science.1196808.

Bayer, T.K., Gustafsson, E., Brakebusch, M., Beer, C., 2019. Future carbon emission from boreal and permafrost lakes are sensitive to catchment organic carbon loads. J. Geophys. Res.: Biogeosciences 124 (7), 1827–1848. https://doi.org/10.1029/2018JG004978.

Bazhin, N.M., 2003. Theoretical consideration of methane emission from sediments. Chemosphere 50, 191–200.

Beaulieu, J.J., DelSontro, T., Downing, J.A., 2019. Eutrophication will increase methane emissions from lakes and impoundments during the 21st century. Nature Communications 10 (1375). https://doi.org/10.1038/s41467-019-09100-5.

Bižić, M., Klintzsch, T., Ionescu, D., Hindiyeh, M.Y., Günthel, M., Muro-Pastor, A.M., et al., 2020. Aquatic and terrestrial cyanobacteria produce methane. Science Advances 6 (3). https://doi.org/10.1126/sciadv.aax5343.

Borges, A.V., Morana, C., Bouillon, S., Servais, P., Descy, J.P., Darchambeau, F., 2014. Carbon cycling of Lake Kivu (East Africa): net autotrophy in the epilimnion and emission of CO2 to the atmosphere sustained by geogenic inputs. PloS One 9 (10). https://doi.org/10.1371/journal.pone.0109500.

Chanudet, V., Harby, A., Descloux, S., Sundt, H., Hansen, B.H., Brakstad, O., Guerin, F., 2011. Gross CO2 and CH4 emissions from the Nam Ngum and Nam Leuk sub-tropical reservoirs in Lao PDR. Science of the Total Environment 409 (24), 5382–5391. https://doi.org/10.1016/j.scitotenv.2011.09.018.

Ciesin, 2005. Gridded Population of the World Version 3 (GPWv3): Population Density Grids. Socioeconomic Data and Applications Center (SEDAC), Center for International Earth Science Information Network, Columbia University; and Centro Internacional de Ag, Palisades, NY.

Cole, J., Prairie, Y., Caraco, N., Mcdowell, W., Tranvik, L., Striegl, R., et al., 2007. Plumbing the global carbon cycle: integrating inland waters into the terrestrial carbon budget. Ecosystems 10, 171–184. Retrieved from papers://147e10c6-99f2-4f05-9c2a-f590f183e1fa/Paper/p.5382.

Deemer, B.R., Holgerson, M.A., 2021. Drivers of methane flux differ between lakes and reservoirs, complicating global upscaling efforts. J Geophys Res Biogeosciences 126. https://doi.org/10.1029/2019jg005600.

Cook, R.D., 1977. Detection of Influential Observation in Linear Regression. Technometrics 19 (1), 15–18. https://doi.org/10.2307/1268249.

Deemer, B.R., Harrison, J.A., Li, S., Beaulieu, J.J., Delsontro, T., Barros, N., et al., 2016. Greenhouse gas emissions from reservoir water surfaces: a new global synthesis manuscript. Bioscience 66 (11), 949–964. https://doi.org/10.1093/biosci/biw117.

DelSontro, T., Giorgio, P.A., Prairie, Y.T., 2018. No longer a Paradox : the interaction between physical transport and biological processes explains the spatial distribution of surface water methane within and across lakes. Ecosystems 21 (6), 1073–1087. https://doi.org/10.1007/s10021-017-0205-1.

DelSontro, T., Boutet, L., St-Pierre, A., del Giorgio, P.A., Prairie, Y.T., 2016. Methane ebullition and diffusion from northern ponds and lakes regulated by the interaction between temperature and system productivity. Limnol. Oceanogr. 61, S62–S77. https://doi.org/10.1002/lno.10335.

DelSontro, T., Beaulieu, J.J., Downing, J.A., 2018. Greenhouse gas emissions from lakes and impoundments: upscaling in the face of global change. Limnology and Oceanography Letters 3, 64–75. https://doi.org/10.1002/lol2.10073.

Demarty, M., Tremblay, A., 2017. Long term follow-up of pCO2 , pCH4 and emissions from Eastmain 1 boreal reservoir , and the Rupert diversion bays , Canada. Ecohydrol. Hydrobiol. 1–12. https://doi.org/10.1016/j.ecohyd.2017.09.001.

DelSontro, T., Kunz, M.J., Kempter, T., Wüest, A., Wehrli, B., Senn, D.B., 2011. Spatial heterogeneity of methane ebullition in a large tropical reservoir. Environ. Sci. Technol. 45 (23), 9866–9873. https://doi.org/10.1021/es2005545.

DelSontro, T., Mcginnis, D.F., Sobek, S., Ostrovsky, I., Wehrli, B., 2010. Extreme methane emissions from a swiss hydropower Reservoir: contribution from bubbling sediments. Environ. Sci. Technol. 44 (7), 2419–2425. https://doi.org/10.1021/es9031369.

Demarty, M., Bastien, J., Tremblay, A., Hesslein, R.H., Gill, R., 2009. Greenhouse gas emissions from boreal reservoirs in Manitoba and Québec, Canada, measured with automated systems. Environ. Sci. Technol. 43 (23), 8908–8915. https://doi.org/10.1021/es8035658.

Dillon, P., Molot, L., 1997. Dissolved organic and inorganic carbon mass balances in central Ontario lakes. Biogeochemistry 36 (1), 29–42. Retrieved from papers://147e10c6-99f2-4f05-9c2a-f590f183e1fa/Paper/p.5370.

Drake, T.W., Raymond, P.A., Spencer, R.G.M., 2018. Terrestrial carbon inputs to inland waters: A current synthesis of estimates and uncertainty. Limnology and Oceanography Letters 3 (3), 132–142. https://doi.org/10.1002/lol2.10055.

ESA-CCI, 2014-2017. The Land Cover CCI Climate Research Data Package (CRDP). European Space Agency (ESA) – Climate Change Initiative (CCI) -. Land Cover Project.

Fearnside, P.M., 2002. Greenhouse gas emissions from a hydroelectric reservoir (Brazil's tucuruí dam) and the energy policy implications. Water Air Soil Pollut. 133, 69–96. https://doi.org/10.1023/a:1012971715668.

Fekete, B.M., Voeroesmarty, C.J., Grabs, W., 2000. Global Composite Runoff Fields on Observed River Discharge and Simulated Water Balances. Complex Systems Research Center, University of New Hampshire. UNH-GRDC Composite Runoff Fields v1.0., (February).

Ferland, M.-E., Prairie, Y.T., Teodoru, C., del Giorgio, P.A., 2014. Linking organic carbon sedimentation, burial efficiency, and long-term accumulation in boreal lakes. J Geophys Res Biogeosciences 119, 836–847. https://doi.org/10.1002/2013jg002345.

Gagnon, L., Bélanger, C., Uchiyama, Y., 2002. Life-cycle assessment of electricity generation options: the status of research in year 2001. Energy Pol. 30 (14), 1267–1278. https://doi.org/10.1016/S0301-4215(02)00088-5.

Galy-Lacaux, C., Delmas, R., Jambert, C., Dumestre, J.-F., Labroue, L., Richard, S., Gosse, P., 1997. Gaseous emissions and oxygen consumption in hydroelectric dams: a case study in French Guyana. Global Biogeochem. Cycles 11 (4), 471–483. https://doi.org/10.1029/97GB01625.

Grinham, A., Dunbabin, M., Gale, D., Udy, J., 2011. Quantification of ebullitive and diffusive methane release to atmosphere from a water storage. Atmos. Environ. 45 (39), 7166–7173. https://doi.org/10.1016/j.atmosenv.2011.09.011.

Gorham, E., Boyce, F., 1989. Influence of lake surface area and depth upon thermal stratification and the depth of the summer thermocline. J. Great Lakes Res. 15, 233–244.

Grinham, A., Dunbabin, M., Albert, S., 2018. Importance of sediment organic matter to methane ebullition in a sub-tropical freshwater reservoir. Sci. Total Environ. 621, 1199–1207. https://doi.org/10.1016/j.scitotenv.2017.10.108.

Günthel, M., Donis, D., Kirillin, G., Ionescu, D., Bizic, M., McGinnis, D.F., Grossart, H.-P., Tang, K.W., 2021. Reply to 'Oxic methanogenesis is only a minor source of lake-wide diffusive CH4 emissions from lakes. Nat. Commun. 12, 1205. https://doi.org/10.1038/s41467-021-21216-1.

Harrison, J.A., Deemer, B.R., Birchfield, M.K., O'Malley, M.T., 2017. Reservoir water-level drawdowns accelerate and amplify methane emission. Environ. Sci. Technol. 51 (3) https://doi.org/10.1021/acs.est.6b03185.

Harrison, J.A., Prairie, Y.T., Soued, C., Mercier-Blais, S., 2021. Year-2020 global distribution and pathways of reservoir methane and carbon dioxide emissions according to the greenhouse gas from reservoirs (G-res) model. Global Biogeochemical Cycles 35. https://doi.org/10.1029/2020GB006888.

Hastings, D.A., Dunbar, P.K., Elphingstone, G.M., Bootz, M., Murakami, H., et al., 1999. The Global Land One-Kilometer Base Elevation (GLOBE) Digital Elevation Model. Version 1.0. NOAA GLOBE Task Team.

Hengl, T., Mendes de Jesus, J., Heuvelink, G.B.M., Ruiperez Gonzalez, M., Kilibarda, M., 2017. SoilGrids250m: global gridded soil information based on Machine Learning. PloS One 12 (2). https://doi.org/10.1371/journal.pone.0169748.

Hertwich, E.G., 2013. Addressing biogenic greenhouse gas emissions from hydropower in LCA. Environ. Sci. Technol. 47 (17), 9604–9611. https://doi.org/10.1021/es401820p.

Hijmans, R.J., Cameron, S.E., Parra, J.L., Jones, G., Jarvis, A., 2005. Very high resolution interpolated climate surfaces for global land areas. Int. J. Climatol. 25, 1965–1978. https://doi.org/10.1002/joc.1276.

IAEA Advisoring Group, 1995. Assessment of greenhouse gas emissions from the full energy chain .~r nuclear" power and other energv sources. In: IAEA Advisory Group Meeting, Vienna, Austria, 26-28 September. Vienna. *1995*.

IAEA Advisoring Group, 1996. Assessment of Greenhouse Gas Emissions from the Full Energy Chain for Hydropower, Nuclear" Power and Other Energy Sources. IAEA Advisory Group Meeting, jointly organized by Hydro-Qu6bec, Hydro-Quebec Headquarter, Montreal. *1996*.

Inglett, K.S., Inglett, P.W., Reddy, K.R., Osborne, T.Z., 2012. Temperature sensitivity of greenhouse gas production in wetland soils of different vegetation. Biogeochemistry 108 (1–3), 77–90. https://doi.org/10.1007/s10533-011-9573-3.

IPCC, 2006. Agriculture, Forestry and Other Land Use - Chapter 4: Forest Land. 2006 IPCC Guidelines for National Greenhouse Gas Inventories, 4. https://doi.org/10.1016/j.phrs.2011.03.002.

IPCC, 2013. 2013 SUPPLEMENT TO THE 2006 GUIDELINES: WETLANDS. THIRTY-SEVENTH SESSION OF THE IPCC. https://doi.org/10.1017/CBO9781107415324.004.

Isidorova, A., Mendonça, R., Sobek, S., 2019. Reduced mineralization of terrestrial OC in anoxic sediment suggests enhanced burial efficiency in reservoirs compared to other depositional environments. J Geophys Res Biogeosciences 124, 678–688. https://doi.org/10.1029/2018jg004823.

Kumar, A., Schei, T., Ahenkorah, A., Caceres Rodriguez, R., Devernay, J.-M., Freitas, M., Hall, D., Killingtveit, Å., Liu, Z., 2011. Hydropower. In: Edenhofer, O., Pichs-Madruga, R., Sokona, Y., Seyboth, K., Matschoss, P., Kadner, S., Zwickel, T., Eickemeier, P., Hansen, G., Schlömer, S., von Stechow, C. (Eds.), IPCC Special Report on Renewable Energy Sources and Climate Change Mitigation. Cambridge University Press, Cambridge, United Kingdom and New York, NY, USA.

Lehner, B., Grill, G., 2013. Global river hydrography and network routing: baseline data and new approaches to study the world's large river systems. Hydrol. Process. 27 (15), 2171–2186.

Lehner, Bernhard, Liermann, C.R., Revenga, C., Vörömsmarty, C., Fekete, B., Crouzet, P., et al., 2011. High-resolution mapping of the world's reservoirs and dams for sustainable river-flow management. Front. Ecol. Environ. 9, 494–502. https://doi.org/10.1890/100125.

Levasseur, A., Mercier-Blais, S., Prairie, Y.T., Tremblay, A., Turpin, C., 2021. Improving the accuracy of electricity carbon footprint: estimation of hydroelectric reservoir greenhouse gas emissions. Renew. Sustain. Energy Rev. 136, 110433 https://doi.org/10.1016/j.rser.2020.110433.

Li, L., Xue, B., Yao, S., Tao, Y., Yan, R., 2018. Spatial–temporal patterns of methane dynamics in Lake Taihu. Hydrobiologia 822, 143–156. https://doi.org/10.1007/s10750-018-3670-4.

Lide, D.R., 1994. In: Handbook of Physics and Chemistry. CRC Press, Boca Raton, U.S.A.

Liikanen, A., Murtoniemi, T., Tanskanen, H., Väisäanen, T., Martikainen, P., 2002. Effects of temperature and oxygen availability on greenhouse gas and nutrient dynamics in sediment of a eutrophic mid-boreal lake. Biogeochemistry 59 (3), 269–286.

Liu, L., Yang, Z.J., Delwiche, K., others, 2020. Spatial and temporal variability of methane emissions from cascading reservoirs in the Upper Mekong River. Water Res. 186, 116319 https://doi.org/10.1016/j.watres.2020.116319.

St Louis, V.L., Kelly, C.a., Duchemin, É., Rudd, J.W.M., Rosenberg, D.M., 2000. Reservoir surfaces as sources of greenhouse gases to the atmosphere: a global estimate. Bioscience 50 (9), 766–775. https://doi.org/10.1641/0006-3568(2000)050[0766:RSASOG]2.0.CO;2.

Marcé, R., Obrador, B., Gómez-Gener, L., Catalán, N., Koschorreck, M., Arce, M.I., et al., 2019. Emissions from dry inland waters are a blind spot in the global carbon cycle. Earth Sci. Rev. 188 (November 2018), 240–248. https://doi.org/10.1016/j.earscirev.2018.11.012.

Mcginnis, D.F., Greinert, J., Artemov, Y., Beaubien, S.E., Wu, A., 2006. Fate of rising methane bubbles in stratified waters : how much methane reaches the atmosphere ?, 111, pp. 1–15. https://doi.org/10.1029/2005JC003183.

Mendonça, R., Kosten, S., Sobek, S., Cole, J.J., Bastos, A.C., Albuquerque, A.L., Cardoso, S.J., Roland, F., 2014. Carbon sequestration in a large hydroelectric reservoir: an integrative seismic approach. Ecosystems 17, 430–441. https://doi.org/10.1007/s10021-013-9735-3.

Mendonça, R., Müller, R.A., Clow, D., Verpoorter, C., Raymond, P., Tranvik, L.J., Sobek, S., 2017. Organic carbon burial in global lakes and reservoirs. Nat. Commun. 8, 1694. https://doi.org/10.1038/s41467-017-01789-6.

NASA, 2008. NASA Surface Meteorology and Solar Energy (SSE) Release 6.0 Data Set (Jan 2008) 22-year Monthly & Annual Average (July 1983 - June 2005). Retrieved from. http://eosweb.larc.nasa.gov/sse/.

Pan, Y., Birdsey, R.A., Fang, I., Houghton, R., Kauppi, ekka E., Kurz, W.A., et al., 2011. A large and persistent carbon sink in the world's forests. Science 333 (August), 988–994.

Peeters, F., Hofmann, H., 2021. Oxic methanogenesis is only a minor source of lake-wide diffusive CH4 emissions from lakes. Nat. Commun. 12, 1206. https://doi.org/10.1038/s41467-021-21215-2.

Prairie, Y.T., Alm, J., Beaulieu, J., Barros, N., Battin, T., Cole, J., et al., 2017a. Greenhouse gas emissions from freshwater reservoirs: what does the atmosphere see? Ecosystems (April), 1–14. https://doi.org/10.1007/s10021-017-0198-9.

Prairie, Y.T., Alm, J., Beaulieu, J., Barros, N., Battin, T., Cole, J.J., del Giorgio, P., DelSontro, T., Guérin, F., Harby, A., Harrison, J., Mercier-Blais, S., Serça, D., Sobek, S., Vachon, D., 2018. Greenhouse Gas Emissions from Freshwater Reservoirs: What Does the Atmosphere See? Ecosystems 21, 1058–1071. https://doi.org/10.1007/s10021-017-0198-9.

Prairie, Y.T., Alm, J., Harby, A., Mercier-Blais, S., Nahas, R., 2017b. Technical documentation, UNESCO/IHA research project on the GHG status of freshwater reservoirs. Version 1.1.

Rasilo, T., Prairie, Y.T., Del Giorgio, P.A., 2014. Large-scale patterns in summer diffusive CH4 fluxes across boreal lakes, and contribution to diffusive C emissions. Global Change Biol. 1, 1–16. https://doi.org/10.1111/gcb.12741.

Raymond, P.A., Hartmann, J., Lauerwald, R., Sobek, S., McDonald, C., Hoover, M., et al., 2013. Global carbon dioxide emissions from inland waters. Nature 503 (7476), 355–359. https://doi.org/10.1038/nature12760.

Rosentreter, J.A., Borges, A.V., Deemer, B.R., others, 2021. Half of global methane emissions come from highly variable aquatic ecosystem sources. Nat. Geosci. 14, 225–230. https://doi.org/10.1038/s41561-021-00715-2.

Rubel, F., Kottek, M., 2010. Observed and projected climate shifts 1901 – 2100 depicted by world maps of the Koppen-Geiger climate classification. Meteorol. Z. 19 (2), 135–141. https://doi.org/10.1127/0941-2948/2010/0430.

Serça, D., Deshmukh, C., Pighini, S., Oudone, P., Vongkhamsao, A., Guédant, P., et al., 2016. Nam Theun 2 Reservoir four years after commissioning : significance of drawdown methane emissions and other pathways. Hydroécol. Appliquée 19, 119–146. https://doi.org/10.1051/hydro/2016001.

Soued, C., Prairie, Y.T., 2020. The carbon footprint of a Malaysian tropical reservoir : measured versus modeled estimates highlight the underestimated key role of downstream processes, 30, pp. 1–22. https://doi.org/10.5194/bg-2019-385. October.

Soued, C., Prairie, Y.T., 2021. Changing sources and processes sustaining surface CO2 and CH4 fluxes along a tropical river to reservoir system. Biogeosciences 18, 1333–1350. https://doi.org/10.5194/bg-18-1333-2021.

Teodoru, C.R., Bastien, J., Bonneville, M.C., Del Giorgio, P.a., Demarty, M., Garneau, M., et al., 2012. The net carbon footprint of a newly created boreal hydroelectric reservoir. Global Biogeochem. Cycles 26 (GB2016), 1–14. https://doi.org/10.1029/2011GB004187.

Thottathil, S.D., Reis, P.C.J., del Giorgio, P.A., Prairie, Y.T., 2018. The extent and regulation of summer methane oxidation in northern lakes. J. Geophys. Res.: Biogeosciences 123 (10), 3216–3230. https://doi.org/10.1029/2018JG004464.

Thottathil, S.D., Reis, P.C.J., Prairie, Y.T., 2019. Methane oxidation kinetics in northern freshwater lakes. Biogeochemistry 143 (1), 105–116. https://doi.org/10.1007/s10533-019-00552-x.

Tranvik, L., Downing, J., Cotner, J., Loiselle, S., Striegl, R., Ballatore, T., et al., 2009. Lakes and reservoirs as regulators of carbon cycling and climate. Limnol. Oceanogr. 54 (6), 2298–2314. Retrieved from papers://147e10c6-99f2-4f05-9c2a-f590f183e1fa/Paper/p.6.

Tremblay, A., Varfalvy, L., Lambert, M., 2008. Greenhouse gases from boreal hydroelectric RESERVOIRS : 15 years OF DATA ?.

Tremblay, Alain, Demers, C., Bastien, J., 2009. GHG Fluxes (CO2, CH4, N2O) before and during the First Three Years after Flooding at the Eastmain 1 Reservoir (Quebec, Canada).

Vachon, D., Prairie, Y.T., 2013. The ecosystem size and shape dependence of gas transfer velocity versus wind speed relationships in lakes. Can. J. Fish. Aquat. Sci. 70 (August), 1757–1764. https://doi.org/10.1139/cfjas-2013-0241.

Vachon, D., Prairie, Y.T., Guillemette, F., del Giorgio, P.A., 2017. Modeling allochthonous dissolved organic carbon mineralization under variable hydrologic regimes in boreal lakes. Ecosystems 20 (4), 781–795. https://doi.org/10.1007/s10021-016-0057-0.

West, W.E., Creamer, K.P., Jones, S.E., 2016. Productivity and Depth Regulate Lake Contributions to Atmospheric Methane. https://doi.org/10.1002/lno.10247.

Wik, M., Thornton, B.F., Bastviken, D., MacIntyre, S., Varner4, R.K., Crill, P.M., 2014. Energy input is primary controller of methane bubbling in subarctic lakes. Geophys. Res. Lett. 41, 555–560. https://doi.org/10.1002/2013GL058510.Received.

Yvon-Durocher, G., Allen, A.P., Bastviken, D., Conrad, R., Gudasz, C., St-Pierre, A., et al., 2014. Methane fluxes show consistent temperature dependence across microbial to ecosystem scales. Nature 507 (7493), 488–491. https://doi.org/10.1038/nature13164. Retrieved from.

Zou, H., Hastie, T., 2005. Regularization and variable selection via the elastic net. Royal Statistical Society 67 (2), 301–320.

Prairie, Y.T., Alm, J., Harby, A., Mercier-Blais, S., Nahas, R., 2017. Technical documentation, UNESCO/IHA research project on the GHG status of freshwater reservoirs. Version 1.1.